AD-A135 481 A TECHNIQUE FOR THE NONDESTRUCTIVE DETECTION OF VOIDS AND COMPOSITION ANO..(U) AEROSPACE CORP EL SEGUNDO CA MATERIALS SCIENCES LAB E P MUNTZ ET AL. 31 AUG 83 1/1

UNCLASSIFIED TR-0083(3726-02)-1 SD-TR-83-65 F/G 11/6 NL

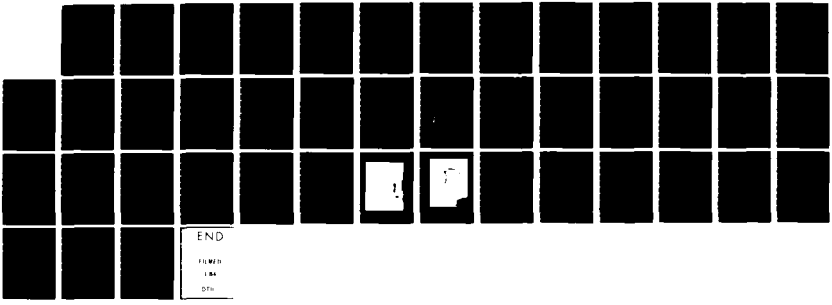

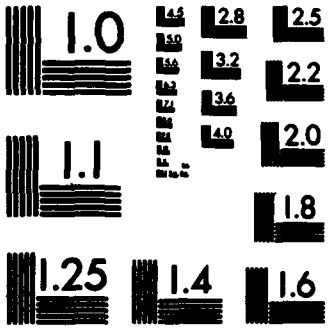

MICROCOPY RESOLUTION TEST CHART
NATIONAL BUREAU OF STANDARDS-1963-A

REPORT NO SD-TR-83-65

(12)

AD-A135 481

A Technique for the Nondestructive Detection of Voids and Composition Anomalies in Metal Matrix Composite Wires Using X or γ Rays

E. P. MUNTZ
Consultant, Aerophysics Laboratory

C. SVE
Aerophysics Laboratory

G. F. HAWKINS
Materials Sciences Laboratory
Laboratory Operations
The Aerospace Corporation
El Segundo, Calif. 90245

31 August 1983

APPROVED FOR PUBLIC RELEASE;
DISTRIBUTION UNLIMITED

Prepared for

NAVAL SURFACE WEAPONS CENTER
White Oak, Silver Spring, Md. 20910

SPACE DIVISION
AIR FORCE SYSTEMS COMMAND
Los Angeles Air Force Station
P.O. Box 92960, Worldway Postal Center
Los Angeles, Calif. 90009

This report was submitted by The Aerospace Corporation, El Segundo, CA 90245, under Contract No. F04701-82-C-0083 with the Space Division, Deputy for Technology, P.O. Box 92960, Worldway Postal Center, Los Angeles, CA 90009. It was reviewed and approved for The Aerospace Corporation by W. P. Thompson, Jr., Director, Aerophysics Laboratory; and L. R. McCreight, Director, Materials Sciences Laboratory. Captain James C. Garcia, WCO, AFSTC, was the project officer for Technology.

This report has been reviewed by the Public Affairs Office (PAS) and is releasable to the National Technical Information Service (NTIS). At NTIS, it will be available to the general public, including foreign nationals.

This technical report has been reviewed and is approved for publication. Publication of this report does not constitute Air Force approval of the report's findings or conclusions. It is published only for the exchange and stimulation of ideas.

James C. Garcia, Captain, USAF
Project Officer

Joseph Hess, GM-15, Director
West Coast Office, AF Space Technology Center

UNCLASSIFIED

SECURITY CLASSIFICATION OF THIS PAGE (When Data Entered)

REPORT DOCUMENTATION PAGE

READ INSTRUCTIONS BEFORE COMPLETING FORM

1. REPORT NUMBER: SD-TR-83-65

2. GOVT ACCESSION NO.: AD-A135 481

3. RECIPIENT'S CATALOG NUMBER:

4. TITLE (and Subtitle): A TECHNIQUE FOR THE NONDESTRUCTIVE DETECTION OF VOIDS AND COMPOSITION ANOMALIES IN METAL MATRIX COMPOSITE WIRES USING X OR γ RAYS

5. TYPE OF REPORT & PERIOD COVERED:

6. PERFORMING ORG. REPORT NUMBER: TR-0083(3726-02)-1

7. AUTHOR(s): E. P. Muntz, Charles Sve, and Gary F. Hawkins

8. CONTRACT OR GRANT NUMBER(s): F04701-82-C-0083

9. PERFORMING ORGANIZATION NAME AND ADDRESS: The Aerospace Corporation, El Segundo, Calif. 90245

10. PROGRAM ELEMENT, PROJECT, TASK AREA & WORK UNIT NUMBERS:

11. CONTROLLING OFFICE NAME AND ADDRESS: Naval Surface Weapons Center, White Oak, Silver Spring, MD 20910

12. REPORT DATE: 31 August 1983

13. NUMBER OF PAGES: 43

14. MONITORING AGENCY NAME & ADDRESS (if different from Controlling Office): Space Division, Air Force Systems Command, Los Angeles, Calif. 90009

15. SECURITY CLASS. (of this report): Unclassified

15a. DECLASSIFICATION/DOWNGRADING SCHEDULE:

16. DISTRIBUTION STATEMENT (of this Report):

Approved for public release; distribution unlimited.

17. DISTRIBUTION STATEMENT (of the abstract entered in Block 20, if different from Report):

18. SUPPLEMENTARY NOTES:

19. KEY WORDS (Continue on reverse side if necessary and identify by block number):

Metal Matrix Composites
Nondestructive testing
X-Rays

20. ABSTRACT (Continue on reverse side if necessary and identify by block number):

A method proposed for the nondestructive testing of metal matrix composite wires is studied theoretically and experimentally. X or γ rays are used to detect the void fraction in these wires by immersing the wires in a bath which has the same linear attenuation coefficient as the matrix material for the x-ray spectrum that is being used. It is concluded that the proposed technique can be expected to detect void fractions of the order of 1% in aluminum matrix, graphite fiber composite wires at a practical linear wire speed.

DD FORM (FACSIMILE) 1473

UNCLASSIFIED

SECURITY CLASSIFICATION OF THIS PAGE (When Data Entered)

PREFACE

The authors thank M.E. Brennan for her expert advice on the computations and R. Ruiz for his design work and assistance with the experiments.

CONTENTS

FIGURES

I. INTRODUCTION

An initial study of a technique proposed for the nondestructive testing of metal matrix composites is the subject of this report. These composites are manufactured in the form of approximately 1/2-mm-diameter "precursor" wires. Larger structures are fabricated by diffusion bonding of lay-ups. Reliable nondestructive quality control indicators of wire integrity have not yet been developed although a number of possibilities are being examined.[1] Testing of the precursor wires is difficult because current manufacturing processes produce wires that may be entirely satisfactory but that vary in cross-sectional geometry, in surface properties, and sometimes in the amount of matrix material that is present. Techniques based on observations of wire resistance, surface emissivity, and sound emission signatures are difficult to interpret because of these characteristics. Wire imaging using x-ray or neutron techniques is also difficult because large lengths of wire must be examined with a resolution in the plane of the wire exceeding 50 line pairs per millimeter. It is difficult to obtain such resolution with techniques that don't use film; also, with these techniques, there is the added burden of a large (approximately 10^5 pieces of information per centimeter of wire) amount of data that must be processed and automatically analyzed using some flaw detection algorithm. The technique investigated in this study uses x or γ rays (neutrons could also be used) but not in an imaging mode. The amount of data that must be processed is reduced by a factor of about 10^4. Additionally, the possibility of very simple flaw, no-flaw signal level criteria is presented so that only minimal data analysis is required.

Consider the situation depicted in Fig. 1. The wire is submerged in and drawn through a liquid bath that has precisely the same linear attenuation coefficient for the radiation being used as a nominally ideal or standard wire, averaged over its cross section. As shown in Fig. 1, the immersed wire is illuminated with x rays, and a detector is placed so that it receives radiation from an area corresponding to the complete cross section of the wire and from a length that is arbitrary but assumed in this study to be one wire

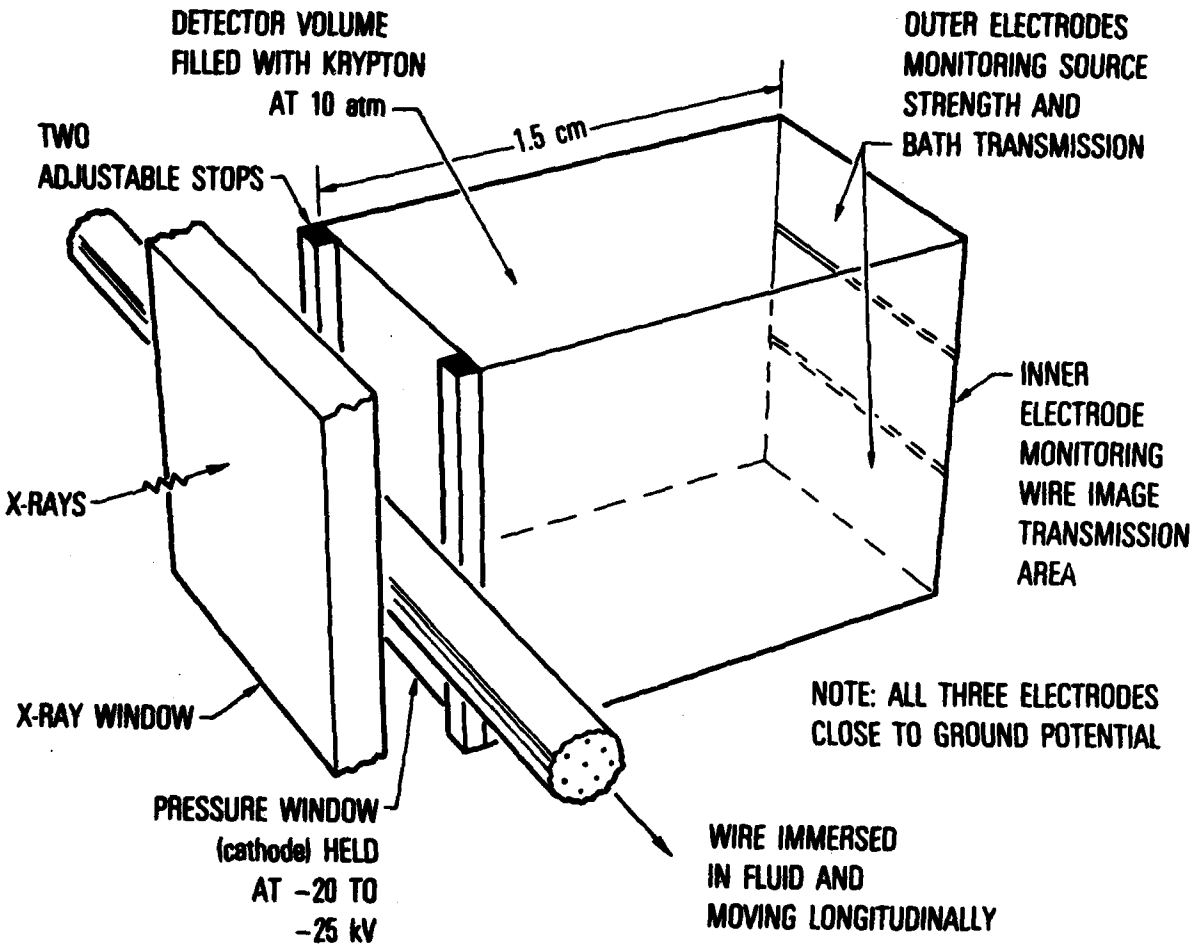

Fig. 1. Sketch of Composite Wire Composition Detector Showing Wire Immersed in Absorbing Fluid

diameter. Immediately adjacent to the first detector, a second balanced detector is used as a reference detector by monitoring x-ray transmission through only the bath material. The signals from the two detectors are compared. If the wire has a standard or ideal composition, both signals will be the same. However, if the wire is not standard, the first detector will give a different signal level than the reference detector. By placing tolerances on the permissible differences between the two signals, a simple method is available for indicating the departure of a wire from its standard composition. Note that the liquid bath automatically adjusts for changes in the wire cross-sectional area and geometry. Thus, the technique is sensitive only to changes in the wire's average composition but not to size or shape variations. In the remainder of the report, we study theoretically and experimentally a number of questions associated with the implementation of this proposed technique.

II. ANALYSIS

The problem of detecting voids or composition anomalies in a composite wire comprised of a matrix material (M) and a fiber (f) is considered. The wire is drawn through a bath that has a linear attenuation coefficient equal to the perfect or standard wire, as shown schematically in Fig. 1. The analysis will be done using aperture theory as it is applied to the study of diagnostic radiographic examinations.[2] The nomenclature used in the analysis is given in Fig. 2. A gas-filled, high pressure ionization chamber that has a relatively high resolution imaging capability is assumed to be the detector.[3-5] The detector selection is dictated by stability, noise injection, and resolution requirements. A more detailed discussion of the detector selection process is presented in another section of this report. In this analysis section, only statistical noise associated with the x-ray photons will be considered. Other noise sources will be investigated in the experimental portion of this work.

The target selected in this study was a length of wire equal to one nominal diameter; thus the target aperture is $A_T \approx D^2$. The image area or aperture at the detector is A_I where

$$A_I = M_T^2 A_T + (M_T - 1)^2 A_{FS} + A_D \tag{1}$$

Here, M_T is the target magnification and is given by

$$M_T = \frac{d_s + L + d_A}{d_s + (L/2)} \tag{2}$$

Because the field illuminated by the x rays is of limited extent and the target is thin, the effects of scattered radiation can be neglected.[6]

The x-ray source will be specified by giving its output at an energy E and a distance of 100 cm as $\dot{\phi}_o(E)$ photons/cm^2 sec keV. For a unit energy interval the fluence rate at the target is hus $\dot{\phi}_o(E)\,(d_s + L/2)^{-2} 10^4$.

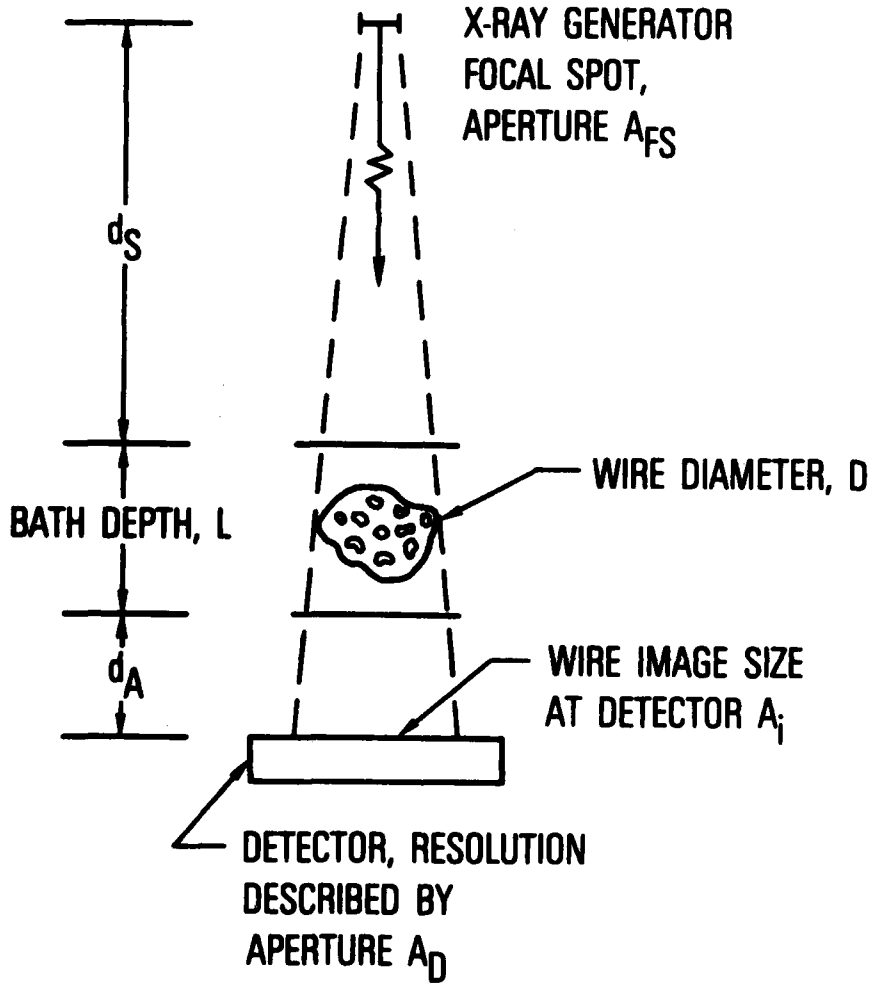

Fig. 2. Schematic Diagram Defining Nomenclature for the Analysis

The primary photon fluence rate in the image plane is

$$\dot{\Phi}_o(E)10^4 \exp[-\mu_{STD}(E)L]/(d_s + L/2)^2 M_T^{\ 2} \tag{3}$$

where $\mu_{STD}(E)$ is the absorption coefficient of the bath and the standard wire. The number of photons in the image area A_i for an exposure time $\langle t \rangle$ is

$$\langle t \rangle \frac{\dot{\Phi}_o(E)10^{\ 4} \exp[-\mu_{STD}(E)L]A_i}{(d_s + L/2)^2 M_T^{\ 2}} = \Phi_I(E)\ A_i \tag{4}$$

For photons of energy E absorbed in a detector, the signal resulting from the absorption is, to a first approximation, proportional to the photon energy. Thus, the photons are weighted by their energy and by the absorption coefficient. The number of events that are recorded is $\Phi_I(E)A_i\eta(E)$, where $\eta(E)$ is the detector absorption efficiency. The standard deviation of absorbed energy is thus $[\eta(E)\Phi_I(E)A_i]^{1/2}\Delta E$, where ΔE is the difference in energy between the energy E and the nearest absorption edge. Contributions from K fluorescence and Auger electrons, which can be important (10 - 30%), are ignored and need not be considered at this point.

If radiation with a spectrum of energies is present, the sum over all energies becomes

$$\left[\int_0^{E_{max}} \langle t \rangle\ \dot{\Phi}_o(E)10^4 A_i \exp[-\mu m(E)L]\eta(E)(\Delta E)^2\ (d_s + L/2)^{-2} M_T^{-2}\ dE\right]^{1/2} \tag{5}$$

For a target of aperture A_T the signal for photons of energy E will be

$$\{\langle t \rangle\ \dot{\Phi}_o(E)\ \exp(-\mu_{STD}L)[\int_{A_T} \Delta\mu(E)\ell\ dA_T]10^4 \Delta E\eta(E)\}/(d_s + L/2)^2 \tag{6}$$

where $\Delta\mu(E)$ is the difference in linear absorption coefficients between a wire and the standard wire. Following Reference 2, we will make the assumption that

$$A_T^{-1} \int_{A_T} \Delta\mu(E)\ell \, dA_T = \Delta\bar{\mu}(E)\ell_{eff}$$

with

$$A_T^{-1} \int_{A_T} \ell dA = \ell_{eff} \approx 0.7D$$

where D is the wire diameter. Integrating over all photon energies results in

$$A_T \int_0^{E_{max}} \langle t \rangle \, \dot{\Phi}_o(E)\exp[-\mu_{STD}(E)L]\Delta\bar{\mu}(E)\ell_{eff}10^4\Delta E\eta(E)(d_s + L/2)^{-2}dE \quad (7)$$

for the absorbed energy associated with the signal.

The signal to noise ratio (SNR) is

$$SNR = \frac{\int_0^{E_{max}} \langle t \rangle \, \dot{\Phi}_o(E)\exp[-\mu_{STD}(E)L]\Delta\bar{\mu}(E)\ell_{eff}A_T10^4(d_s + L/2)^{-2}\Delta E\eta(E)dE}{\{\int_0^{E_{max}} \langle t \rangle \, \dot{\Phi}_o(E)10^4(d_s + L/2)^{-2}M_T^{-2}A_i\exp[-\mu_{STD}(E)]L(\Delta E)^2\eta(E)dE\}^{1/2}} \quad (8)$$

In order to relate this expression to the normally measured output of an x-ray tube $\dot{\varepsilon}_M$ in Roentgens per second (R/s), we have

$$\dot{\varepsilon}_M = \frac{10^4}{d_M^2} \int_0^{E_{max}} \dot{\Phi}_o(E) \frac{(\mu_{en}/\rho)_{AIR}}{K} E(1.6 \times 10^{-9})dE \quad (9)$$

where d_m is the distance at which $\dot{\varepsilon}_M$ is measured. The energy absorption coefficient for air $[(\mu_{en}/\rho)_{AIR}]$ was obtained from Reference 7. The form of $\dot{\Phi}_o(E)$, which has units of photons/sec cm^{2}keV, is assumed to be Kramer's expression,[8]

$$E\dot{\Phi}_o(E) = \dot{C}(E_{max} - E)\exp -[\mu_{INH}(E)\ell_{INH}] \tag{10}$$

Here, $\mu_{INH}(E)$ will be assumed to be for aluminum and ℓ_{INH} will depend on the x-ray generator. A typical value for ℓ_{INH} may be 0.5 mm,[9] so

$$E\dot{\Phi}_o(E) = C(E_{max} - E)\exp -\mu_{INH}(E)0.05 \tag{11}$$

and $\dot{C}$, which has units of photons/cm^2 sec keV, can be evaluated as

$$\dot{C} = \frac{d_M^2}{10^4}\,\dot{\varepsilon}_M K/\int_0^{E_{max}} (E_{max} - E)\exp[-\mu_{Al}(E)0.05]\,(\mu_{en}/\rho)_{AIR}(1.6 \times 10^{-9})dE \tag{12}$$

Here, K is the energy absorbed in 1 gm of air that represents 1 R (87 ergs, and 1 keV = 1.6×10^{-9} ergs).

It is of interest to estimate the current that the detector produces. If it is assumed that the area of one electrode segment is A_l and that approximately 0.024 keV is required for the creation of an electron-ion pair in krypton,[10] we get, assuming $A_l \approx M_T^2 A_T$

$$i = A_l \int_0^{E_{max}} \dot{\Phi}_o(E)\,\frac{\exp\,[-\mu_{STD}(E)L]}{(d_s + L + d_A)^2}\,10^4(\Delta E/0.024)\eta(E)(1.6 \times 10^{-19})dE \tag{13a}$$

Also, the actual signal current (in amperes) corresponding to expression (7) and assuming $A_l \approx M_T^2/A_T$, is

$$i_s = A_l \int_0^{E_{max}} \dot{\Phi}_o(E)\,\frac{\exp[-\mu_{STD}(E)L]}{(d_s + L + d_A)^2}\,\Delta\bar{\mu}(E)\,\ell_{eff}10^4(\Delta E/0.024)\eta(E)(1.6 \times 10^{-19})dE \tag{13b}$$

It is necessary to determine $\Delta\bar{\mu}(E)$, which requires some assumptions about the nature of the anomalies in the composite wires. After studying several sample wire cross sections, we found that in many cases the matrix material simply did not penetrate the fiber bundle. The fibers appear to be distributed in a configuration independent of the presence or lack of matrix material. Thus, the anomalies appeared to be best approximated by a model that assumes an air void or simple lack of matrix material with the volume fractions (X) related such that

$$X_M + X_V = X_{MSTD} \tag{14a}$$

and

$$X_f = X_{fSTD} \tag{14b}$$

The subscript STD represents the ideal or standard composite wire. For this situation, if $\bar{\mu}_W$ (E) refers to a wire that is being tested,

$$\Delta\bar{\mu}(E) = \bar{\mu}_{STD} - \bar{\mu}_W = X_V \mu_M(E) \tag{15}$$

Another possibility for modeling an anomalous wire is that the composition changes, but there are no voids. For this case

$$\bar{\mu}_W(E) = \frac{\mu_M(E)(\rho_W - \rho_f)}{(\rho_M - \rho_f)} + \frac{\mu_f(E)(\rho_M - \rho_W)}{(\rho_M - \rho_f)} \tag{16}$$

Note that the standard wire is such that

$$\bar{\mu}_{STD}(E) = \frac{\mu_M(E)(\rho_{STD} - \rho_f)}{(\rho_M - \rho_f)} + \frac{\mu_f(E)(\rho_M - \rho_{STD})}{(\rho_M - \rho_f)} \tag{17}$$

Still another possibility is that the wires, because of their construction, have a fixed amount of fiber but varying amounts of matrix material, along with possible voids. In this case there is no readily specified "standard" wire, and it is appropriate for the bath to have an

absorption coefficient equal to the matrix material absorption coefficient. We use the same image area as in the previous analysis. (Actually we might want to look at slightly larger image areas to ensure that all of the wire material is always in view.) The detection task is to observe voids in a matrix material in the presence of the fibers. The transmission through the matrix material with a volume fraction of fibers X_f' (and $X_M' = 1 - X_f'$) is given by

$$\bar{\mu}(E) = \mu_M(E)X_M' + \mu_f(E)X_f' \tag{18}$$

Here, the primes indicate that the amount of matrix material or its equivalent bath material is determined by the bath dimension L and not simply by the nominal wire diameter. We will use superscript primes to denote this case for the volume fraction. The basic photon fluence that provides the noise is the same as in expression (3), except that $\bar{\mu}(E)$ replaces $\mu_{STD}(E)$ and expression (5) becomes

$$\left\{\int_0^{E_{max}} \langle t\rangle\, \dot{\Phi}_o(E)\exp[-\bar{\mu}(E)L]A_i M_T^{-2} 10^4 (d_s + L/2)^{-2} (\Delta E)^2 \eta(E)dE\right\}^{1/2} \tag{19}$$

The signal is

$$\int_0^{E_{max}} \langle t\rangle\, \dot{\Phi}_o(E)\exp[-\bar{\mu}(E)L]\Delta\bar{\mu}(E)L10^4(d_s + L/2)^2 \Delta E\eta(E)dE \tag{20}$$

The $\Delta\bar{\mu}(E)$ can be determined from Eq. (14), with X appropriate to the present problem (i.e., based on both matrix and matrix equivalent materials.) Thus we have

$$\Delta\bar{\mu}(E) = \mu_M X_v' \tag{21}$$

Again note that the X_v' is based on the bath depth and not on the wire diameter.

Other target models are possible and will be considered in a later paper if appropriate. Information on the nature of the defects might also be obtained by using two x-ray beams with different average energies.[11]

III. CALCULATED RESULTS

Using the expressions developed in the preceding section, we have made calculations for SNR [Eq. (8)] and current [Eq. (13)] with the target model given by Eq. (21). The composite was assumed to be graphite fibers in an aluminum matrix. The wire void fraction X_v was assumed to be 0.01, the bath thickness 0.125 cm, and the nominal wire diameter 0.0625 cm. The detector, as represented by $\eta(E)$ and $\Delta(E)$, was assumed, for some of the calculations, to be a perfect detector with $\eta(E) = 1$ and $E_K = 0$. For other calculations, a high pressure krypton or Freon detector was modeled by having $\eta(E) = 1$ but E_K = 14.0 keV. The carbon was assumed to have a density $\rho_c = 2.00$ gm/cm^3, and the aluminum $\rho_{Al} = 2.70$ gm/cm^3. The mass absorption coefficients used for carbon and aluminum were obtained from Reference 12. The discrete values from Reference 12 were fitted with polynomials for purposes of the computations.

The calculations were all done with the assumption that the output of the x-ray source resulted in a measured exposure of 1 R/sec at 100 cm. These values substituted into Eq. (12) provide a $\dot{C}$ for each kVp or E_{max} used in the calculations. The resultant values of SNR and current must be adjusted to account for the actual output of x-ray sources. A typical industrial x-ray source with a nominal 0.5 mm focal spot, no liquid cooling, tungsten target, and 0.51 mm of Al added filtration (in order to match the 0.50 mm inherent filtration assumed in the calculations since this source had a beryllium window) has an increasing output with increasing E_{max} (kVp), as shown in Fig. 3. This particular source will be used to convert the calculated SNR's and currents to predictions for a realistic composite wire quality control device.

With the conditions just described, using the calculated SNR/$(R_{100})^{1/2}$ results (note $\dot{t}_{100}$ $\langle t \rangle \equiv R_{100}$) shown in Fig. 4, we have predicted the electrode current, based on the source of Fig. 3, for a high pressure gas ionization detector. The results are shown in Fig. 5. Note that all the calculations are for an x-ray source to target distance of 10 cm. Other geometric parameters have been varied, with d_A going from 0.1 to 10 cm and the

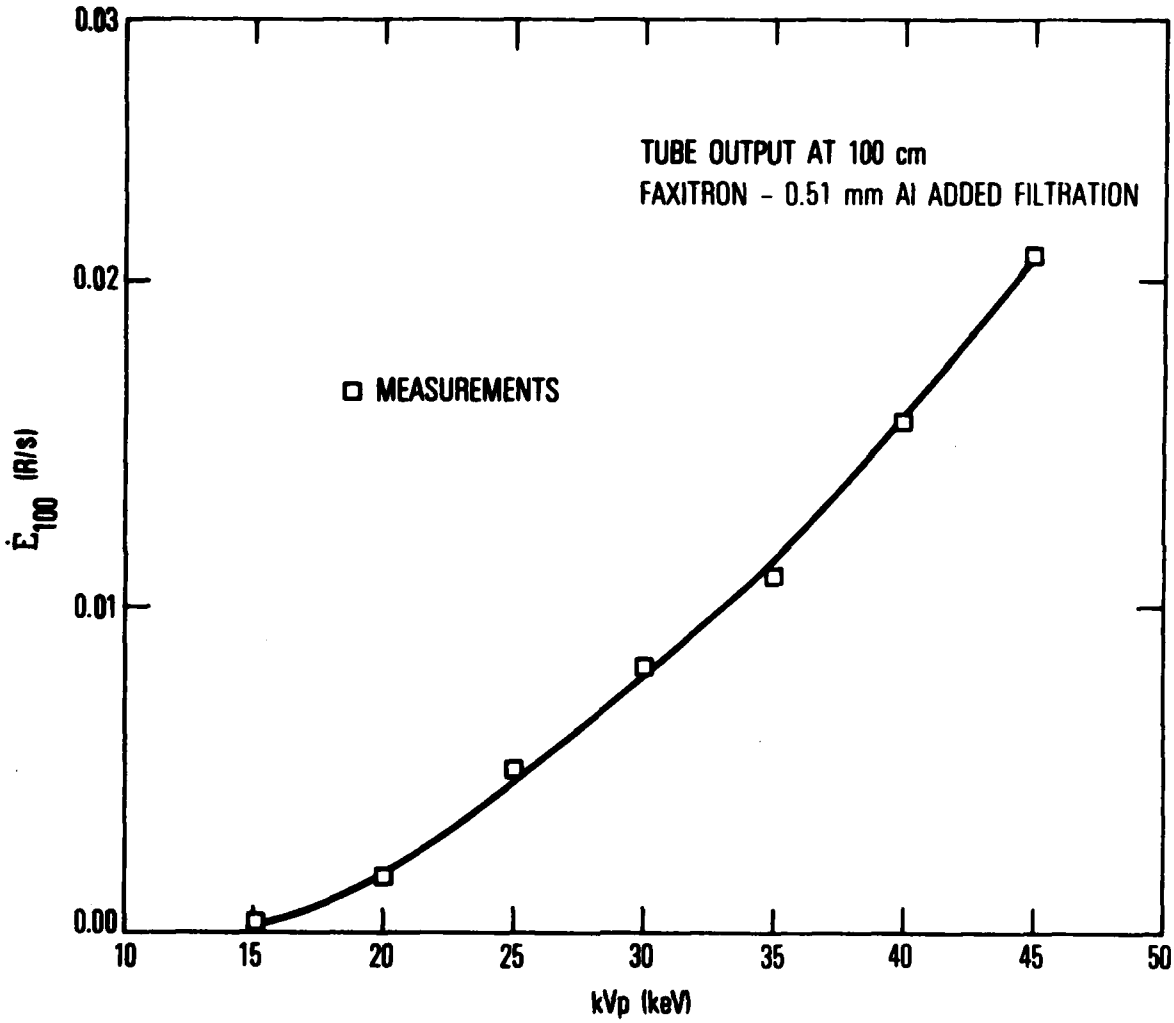

Fig. 3 Experimental Output of Faxitron X-Ray Unit in Roentgens/sec at 100 cm

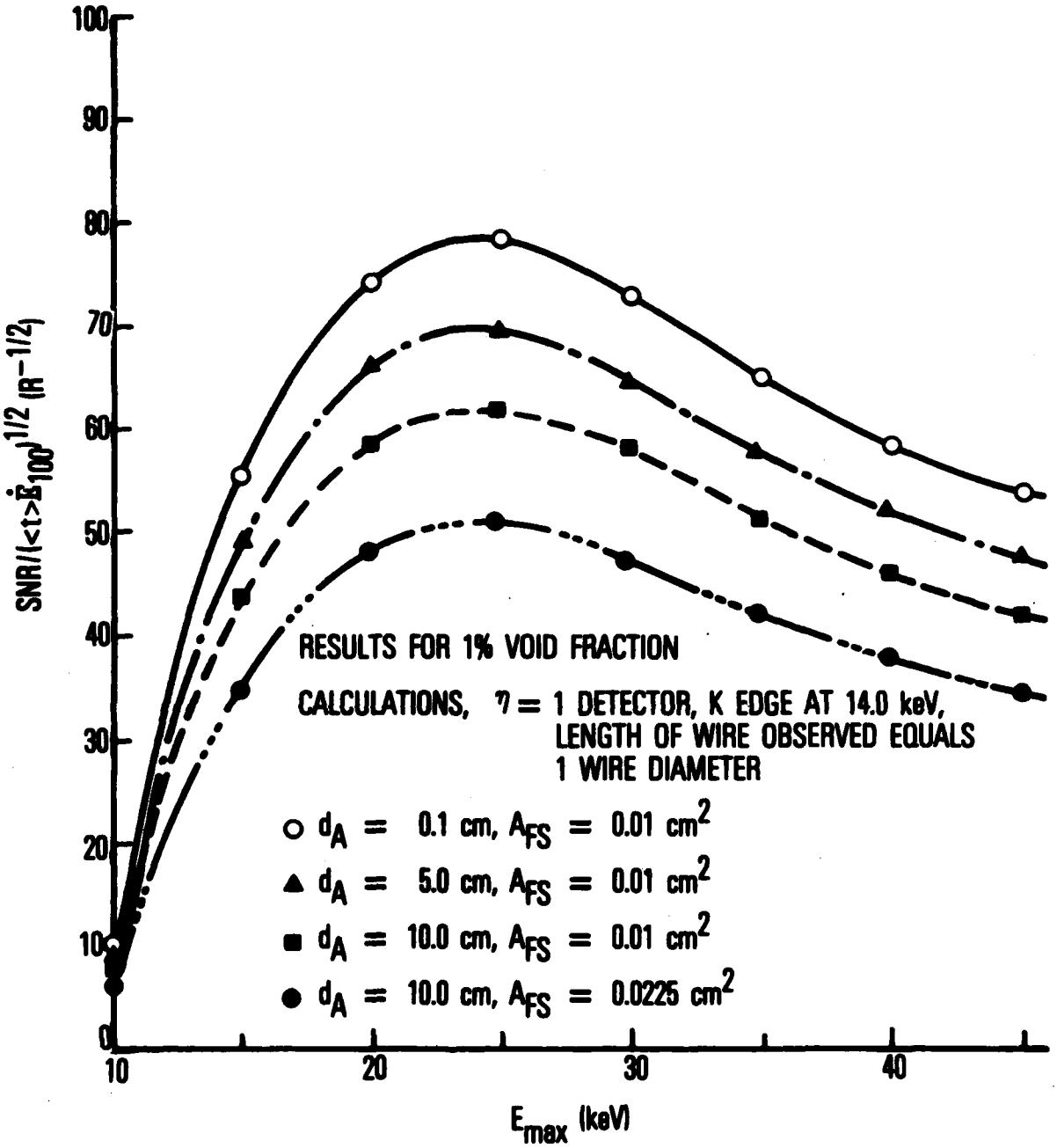

Fig. 4. Calculated SNR per Unit Exposure of 1% Void Fraction in a Composite Wire

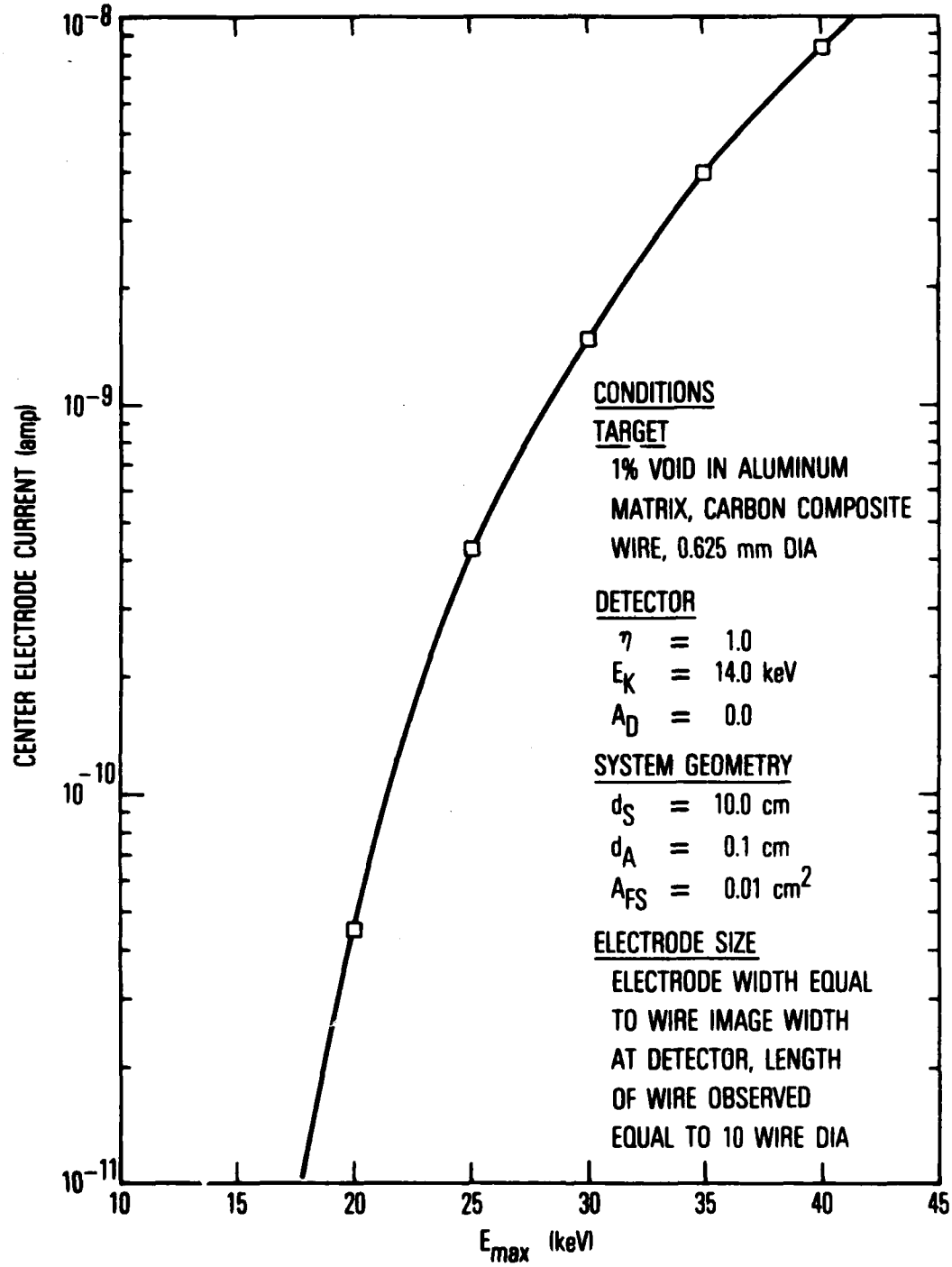

Fig. 5. Calculated Center Electrode Current of Composite Wire Monitor for Exposure to Source in Fig. 3, but d_s = 10 cm

focal spot aperture A_{FS} taking values of 0.01 and 0.0225 cm^2. The length of wire observed for the results in Fig. 5 was assumed to be 10 wire diameters (6.25 mm).

The SNR results in Fig. 4 indicate that there is an optimum in $SNR/R_{100}^{1/2}$ at an E_{max} of approximately 26 keV. However, the picture is different when the change of tube output with E_{max} (Fig. 3) is taken into account. A typical electrode current curve is shown in Fig. 5, it exhibits a monotonic increase with voltage. SNR and signal current [Eq. (13b)] are shown in Fig. 6. The SNR monotonically increases with increasing E_{max} to 45 keV, which was the limit of the calculations, although after about 30 keV the increases are not very significant. Conversely, the signal current increases significantly throughout the voltage range considered. The usable lower limit to E_{max} will be determined by system electronic noise or detector absorption efficiency, with system noise likely representing the most serious problem; however, this limit will depend on the details of the injected noise characteristics. This question will be discussed further in the section of this report on experimental results. For our example, the signal current is of the order of $X_v \mu_{al} L$ ($\approx$0.005 for a 20-keV average photon energy and X_v = 0.01) times the total detector current. In the experimental section, the signal currents will be compared to observed detector system dark currents.

In the analysis of this section, it was assumed that the bath had an absorption coefficient equal to the nominally standard wire or in some cases to the matrix material. For a monochromatic x-ray beam, this assumption presents no difficulty. However, for the case of polychromatic beams, in order to be rigorously correct, the assumption requires an exact match of absorption coefficients over a range of photon energies. In general, this match will not occur because the bath will be conveniently a liquid solvent with an added high atomic number solute. A question then arises concerning the modeling. Consider as an example the target model that matches the bath to the absorption coefficient of matrix material. Is there a spurious signal if the amount of matrix material changes but the wire is otherwise sound? For the case of graphite fiber-aluminum matrix wire, if the aluminum volume fraction changes significantly but the void fraction (relative to the bath depth)

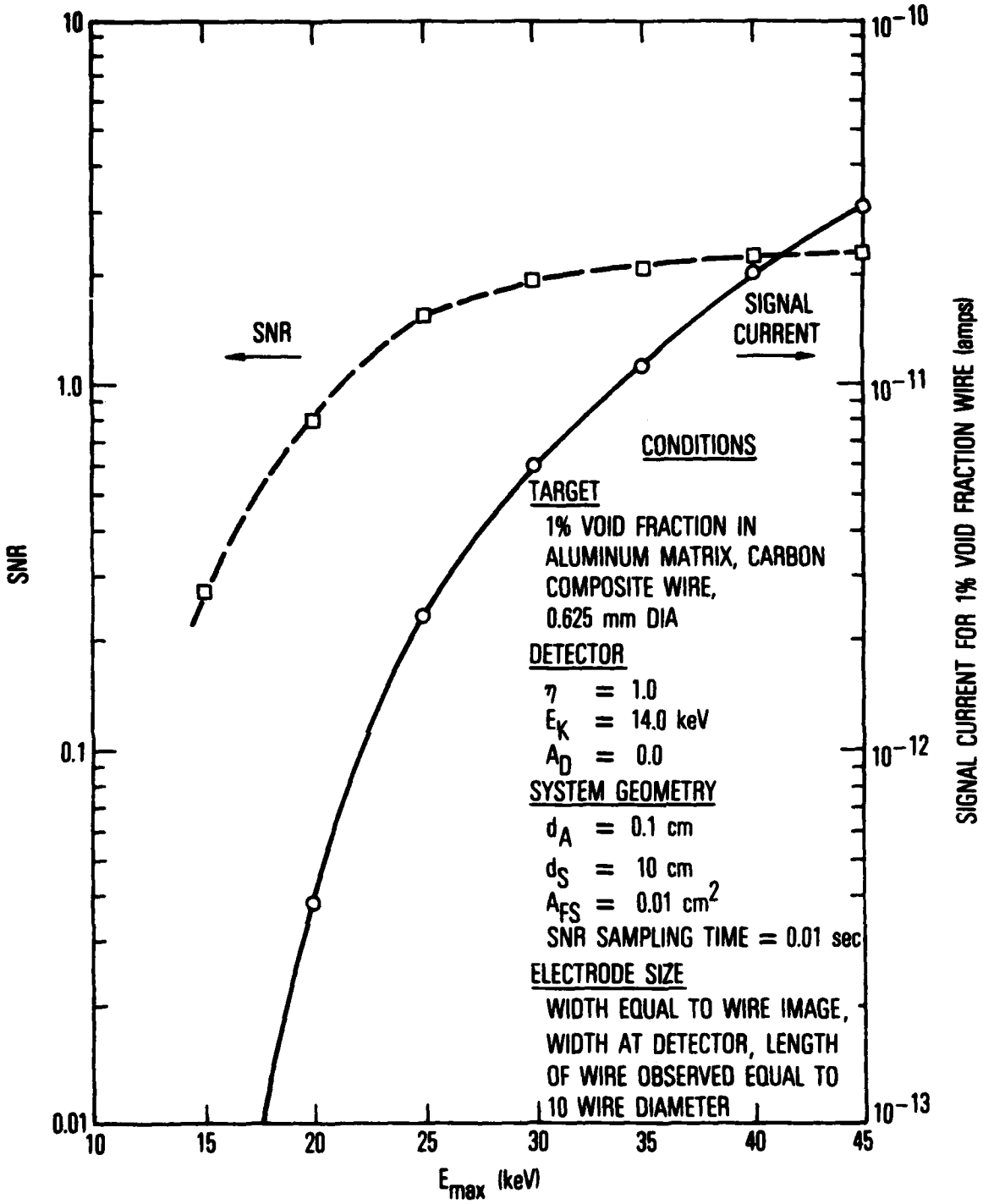

Fig. 6. SNR and Signal Current of Composite Wire Monitor for Exposure to Source in Fig. 3, but d_s = 10 cm

remains constant, the question is whether the aluminum volume fraction change will cause an indication of a void fraction change. This question is addressed in the following paragraphs; it turns out that aluminum volume fraction changes do not present a problem and there is in fact some advantage in having slightly mismatched absorption coefficients as a function of photon energy.

In order to answer this question, it is best to do specific calculations. We have chosen to examine the case of an aluminum matrix-graphite fiber wire in a bath that matches the aluminum absorption coefficient. For the bath, water with varying concentrations of iodine is assumed. Conveniently, the iodine comes bound in organic, water soluble compounds that have been developed for medical diagnostic x-ray applications. In the calculations we have done in this section, which are only for illustrative purposes, the small effect of the binding material has been ignored. We have also chosen to stay below the K edge of iodine for the maximum photon energies used in these particular calculations.

It is of interest to look at the general problem of matching absorption coefficients for a polychromatic beam. Consider the sketch in Fig. 7. In this figure, if $\mu_B(E)$ and the $\mu_W(E)$ are the linear absorption coefficients for the bath and standard wire (or matrix material), respectively, two possibilities [apart from the trivial one of $\mu_B(E) \equiv \mu_W(E)$] present themselves and are shown in the figure. For Fig. 7(a), the bath curve drops off more slowly than the wire curve. The bath curve can be moved vertically by changing the amount of solute without dramatic shape or slope changes, at least over a reasonable range of photon energies. In this situation the crossing energy or monochromatic beam energy where $\mu_W(E) = \mu_B(E)$ decreases as the solute concentration increases. Polychromatic beams will behave in a qualitatively similar manner with the beam energy for balanced attenuation decreasing as the solute concentration increases. If the absorption coefficient curves are similar to those in Fig. 7(b), the reverse happens, and the balance energy increases as the solute concentration increases.

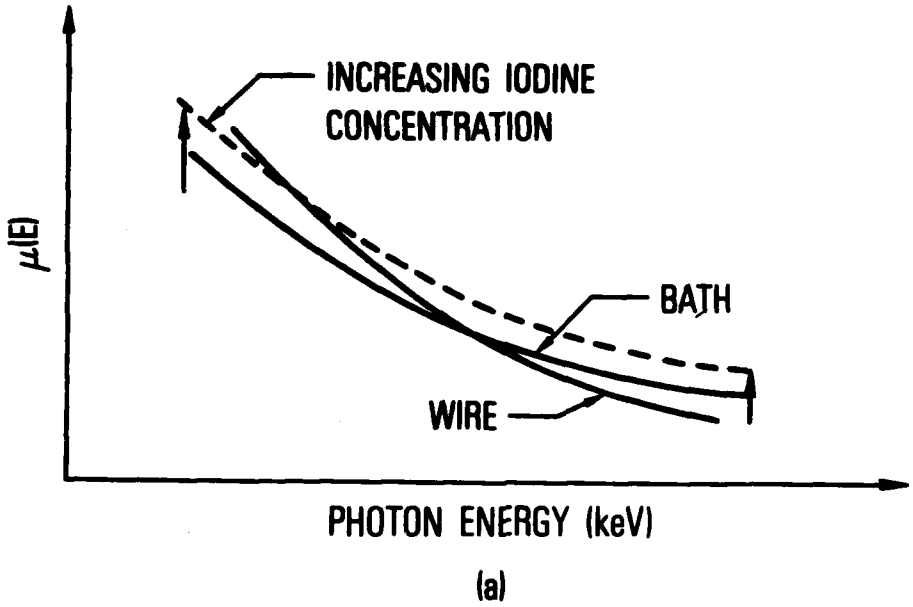

(a)

Fig. 7(a). Effect of Increasing Iodine Concentration of Bath on the Energy Where the Bath and Wire Have the Same Absorption Coefficient. In this case, the bath absorption curve has a slower drop-off with energy than the wire.

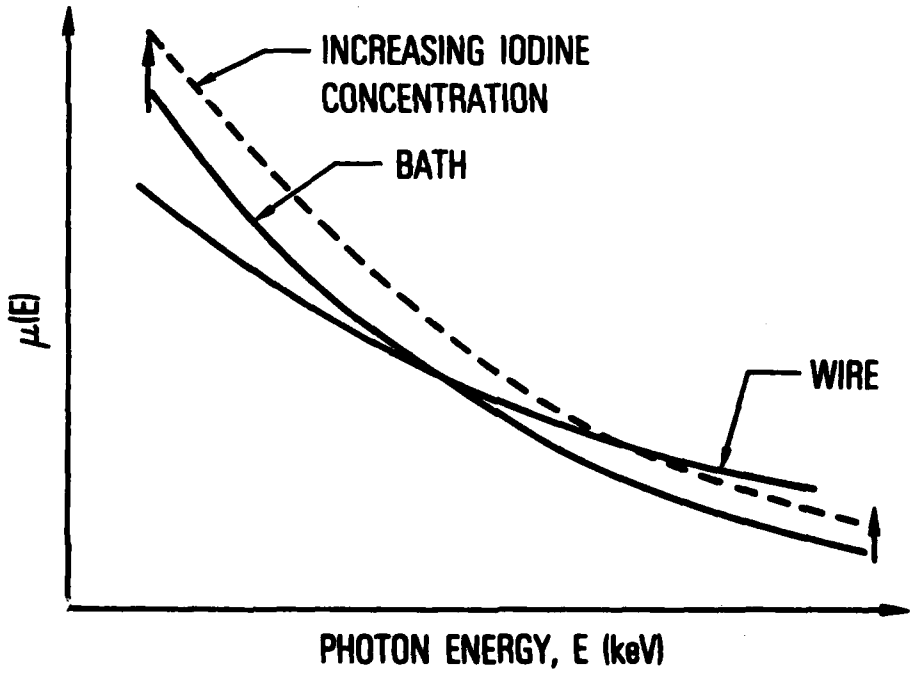

(b)

Fig. 7(b). Same as 7(a), but for Case Where Bath Has a Steeper Drop in Absorption Coefficient than the Wire

As a specific case, consider the question of aluminum in a bath. The volume fraction of aluminum and bath are X'_{Al} and X'_B, respectively. A linear attenuation coefficient is defined for the aluminum-bath mixture as

$$\overline{\mu(E)} = \mu_{Al}(E)X'_{Al} + \mu_B(E)X'_B \tag{22}$$

The corresponding energy absorbed in the detector is

$$\Sigma = A_i \int_0^{E_{max}} \langle t \rangle \dot{\Phi}_o \frac{(E)\, e^{-\bar{\mu}(E)L}(\Delta E)\eta(E)}{10^{-4}(d_s + L + d_A)^2}\, dE \tag{23}$$

Now the bath attenuation coefficient can be written as

$$\mu_B(E) = \rho_S\left[\frac{\mu(E)}{\rho}\right]_S + \rho_H\left[\frac{\mu(E)}{\rho}\right]_H \tag{24}$$

where the subscripts S and H refer to solvent and heavy solute, respectively. If we require that the detector's absorbed energy is unchanging for small changes in X'_{AL} (and hence X'_B since $X'_{AL} + X'_B = 1$), the derivative with respect to X'_{AL} of the absorbed energy ratioed to the absorbed energy is

$$\frac{1}{\Sigma}\frac{\partial \Sigma}{\partial X'_{Al}} = 0 \tag{25}$$

This equation, which can be derived from Eq. (23), can be solved numerically to find ρ_H as a function of E_{max}. For an iodine in water bath, the iodine concentration is shown in Fig. 8 as a function of the E_{max} required to satisfy Eq. (25). Note the decreasing E_{max} as ρ_H is increased. As can be seen, the E_{max} required for balance is quite sensitive to ρ_H.

In order to evaluate the proposed bath-target balance for polychromatic beams with finite changes in X'_{Al}, further computations have been made. In these computations, the detector signal at varying X'_{Al} ratioed to the signal at $X'_{Al} = 0.5$ was calculated for a $\rho_I = 0.340$ gm/cm^3 and $E_{max} = 23.825$ keV.

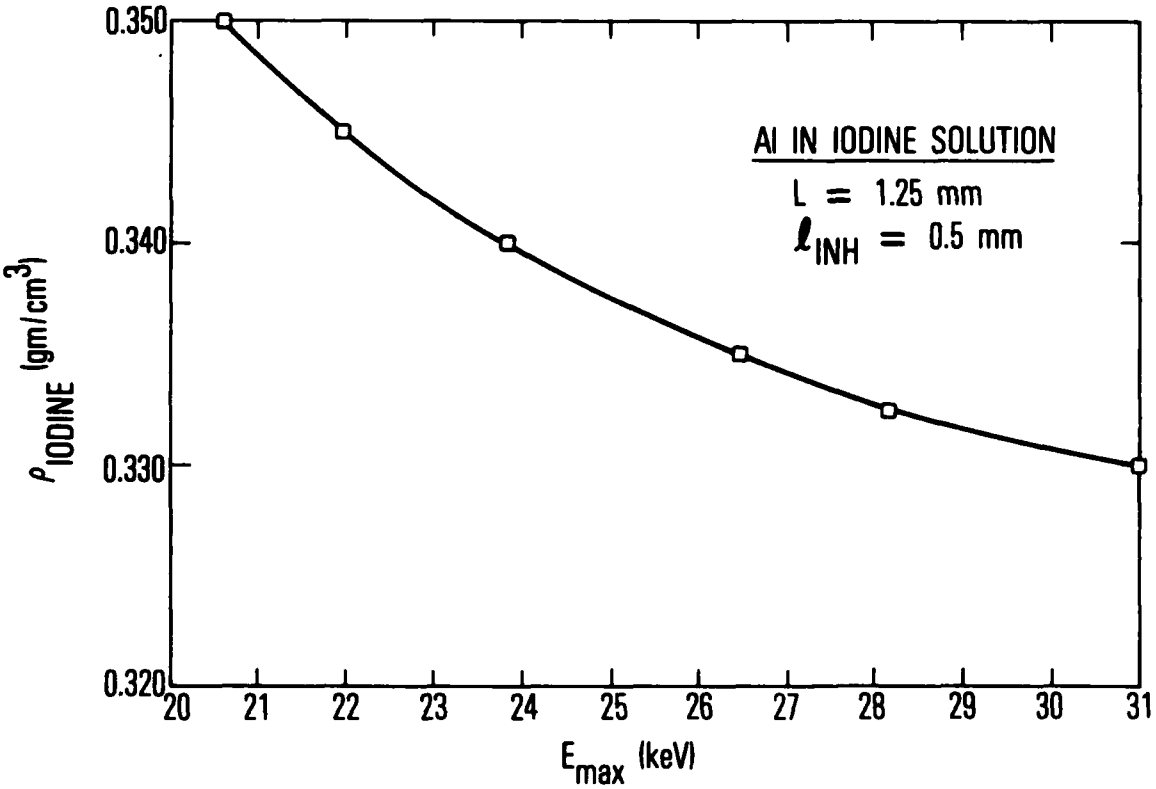

Fig. 8. Balance E_{max} for Aluminum in an Iodine/Water Bath

The results are shown in Fig. 9, which reveals a very small change in detector signal for substantial changes in X_{Al}.

From the preceding work, it was concluded that it is advantageous to have slightly different μ vs E slopes for the bath and the material that is being matched. This permits the use of E_{max} to fine tune the matching. It was also concluded that there should be no significant effect resulting from the normal differences in composite wire sizes (± 20%).

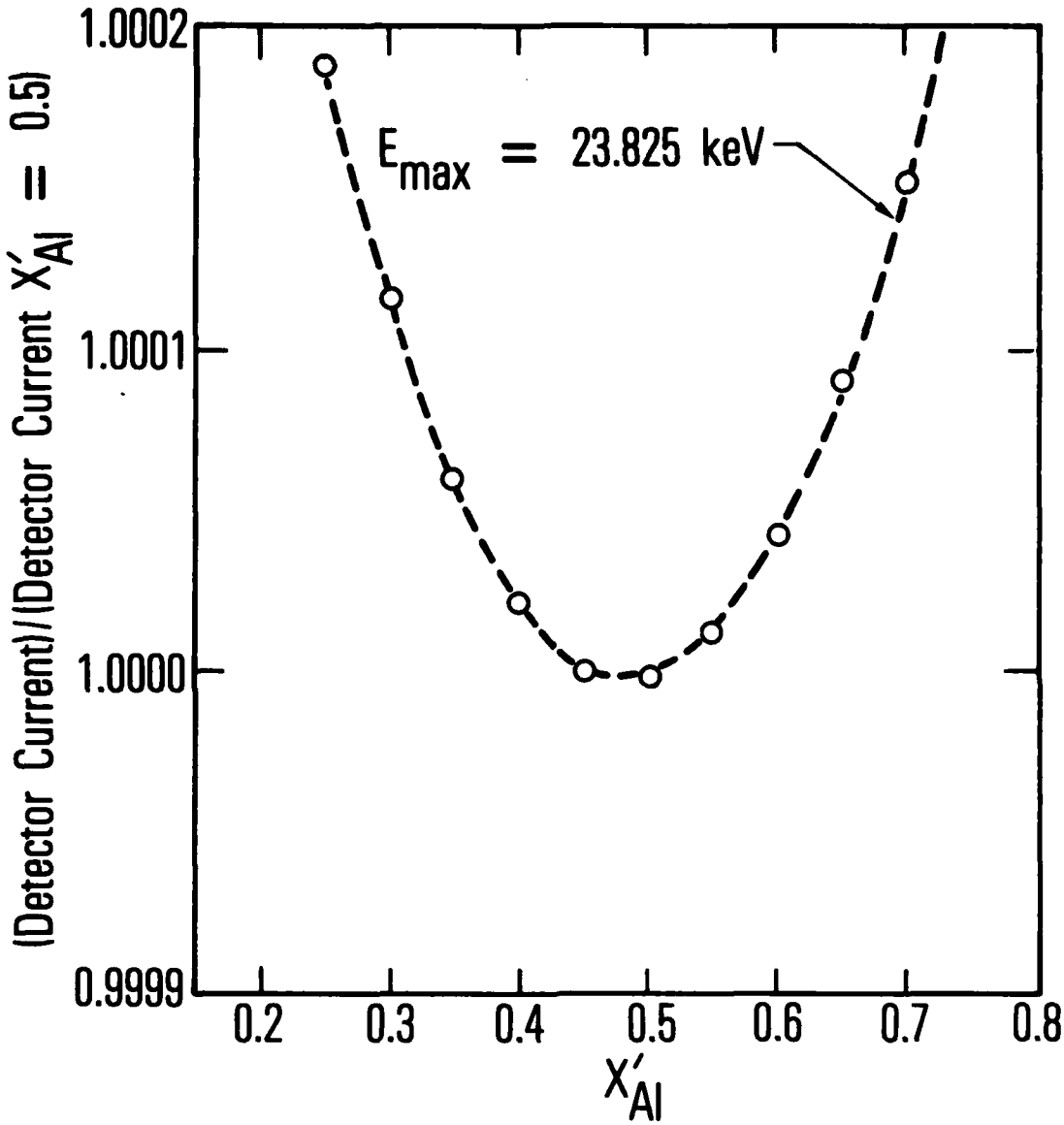

Fig. 9. Fractional Change in Center Electrode Current for Changes in the Aluminum Volume Fraction in the Bath

IV. DETECTOR SELECTION

As is evident from the calculations presented in the previous section, the detector system must provide good stability and low noise injection. Because of the small anomalies that are to be detected, only errors less than about one part in ten thousand should be introduced by the detector system. This problem is similar to the situation in some types of x-ray computed axial tomography scanners where lack of stability leads to image artifacts, and significant detector noise injection is diagnostically unacceptable. For the types of scanners most sensitive to artifacts, high pressure ionization chambers have been selected by their manufacturers because of stability and low noise injection. The present application has an additional requirement for a certain amount of imaging or resolution capability, in order to resolve the wire images so that there is negligible cross talk between the electrode sensing the wire transmission and the reference electrodes. High pressure imaging ionization chambers have been developed for medical x-ray diagnostic purposes over the past several years and typically may have a detector aperture of 0.03 mm^2.[4,14] For our initial development work in this study, we have chosen to use imaging ionization chambers with a segmented sensing electrode. The imaging chamber works in the manner shown in Fig. 1. X-ray photons are absorbed in the imaging gas which, for our purposes, will be krypton or Freon 13B1 (containing bromine). The photoelectrons and Auger electrons that are produced as a result of the absorption events have a short range in the high pressure gas and produce a relatively large number of electron-ion pairs. The electric field causes the electrons (or more frequently, negative ions) and positive ions to migrate to opposite electrodes. Very little lateral diffusion takes place if the electric field is greater than about 1500 V/mm, so the x-ray intensity distribution is reflected in the charge density distribution at either electrode. For this study, we are interested in the imaging characteristic only because it is necessary to have a well defined wire image area, so that the inner electrode in Fig. 1 can be made nearly equal to the diameter of the magnified image of the wire at the detector. If the inner electrode is made any larger, the SNR is reduced proportionately.

In addition to the electrode configuration shown in Fig. 1, there is the possibility of an equivalent but geometrically different arrangement, such as that shown in Fig. 10. This configuration produces the same information as that of Fig. 1, provided the total inner electrode current is only from the image area. However, the configuration requires significantly less potential difference between the electrodes because the electrode gap is only 3 mm compared to 1 to 2 cm for the first configuration. The gas depth required along the x-ray beam direction of propagation is dictated by the pressure (conveniently, 10 atm) and the x-ray energy. Typically, 1 to 2 cm will provide practically complete absorption below 25 keV.

Because we were concerned with such noise injection possibilities as leakage currents, we decided to try the second electrode configuration. This configuration permits the use of a maximum potential of about 4000 to 5000 V across the electrodes compared to approximately 25,000 V for the first geometry.

A photograph of the detector used in our preliminary experiments is shown in Fig. 11. This detector proved to be quite satisfactory with an observed leakage current of 10^{-12} A. The electrodes are vapor deposited gold on glass slides with a 3-mm gap maintained between the electrodes. Care was taken to insulate the electrode leads so that only well defined areas of the electrodes were active. The three segmented electrodes each had a width of 1 mm. In Fig. 11 the x-rays would come from below and pass between the two rod-mounted glass plates, which are the substrates for the electrodes. The plates and their electrodes are normally inside the cylindrical pressure chamber shown in Fig. 12. The lower metal flange in Fig. 11 is inverted in actual use and is the upper flange of the pressure cylinder or detector chamber of Fig. 12.

Mounted on top of the detector chamber in Fig. 12 is the bath and test wire feed-throughs which are the small tubes forming a concave upward curve on either side of the bath housing. The bath and wires can be translated normal to the wires' axes by the micrometer shown in Fig. 12.

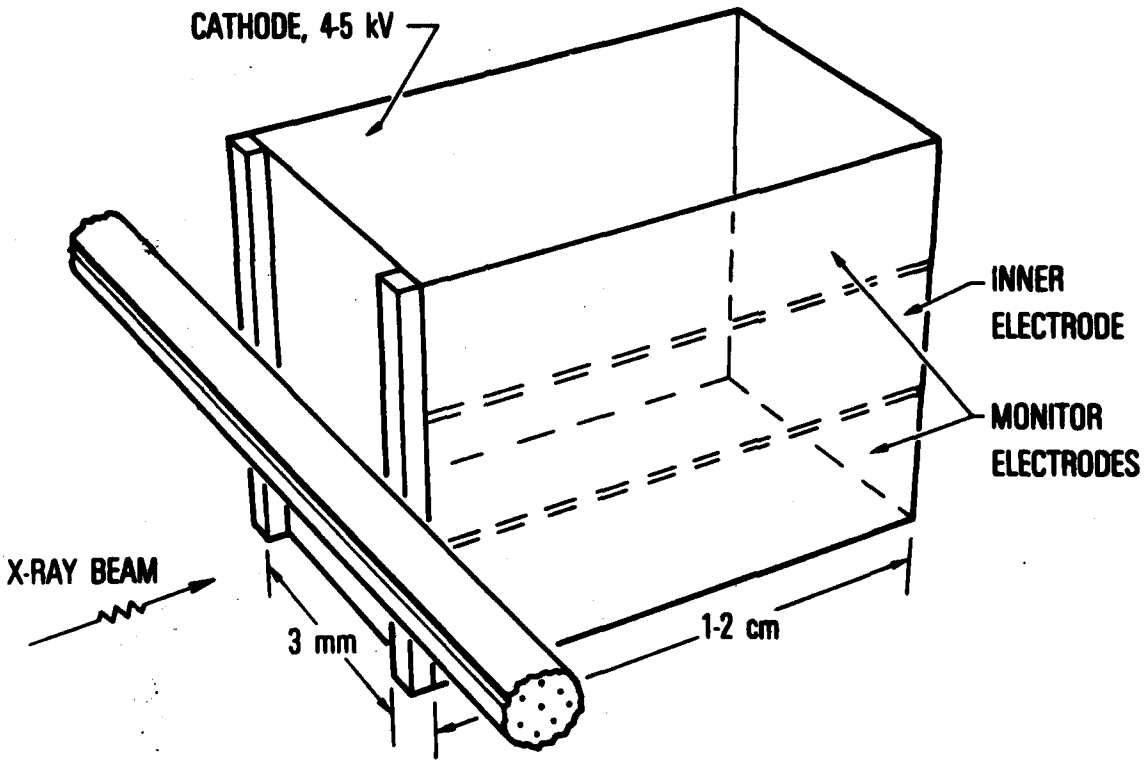

Fig. 10. Sketch of Alternative Electrode Configuration that Permits Lower Electrode Potentials than Configuration in Fig 1

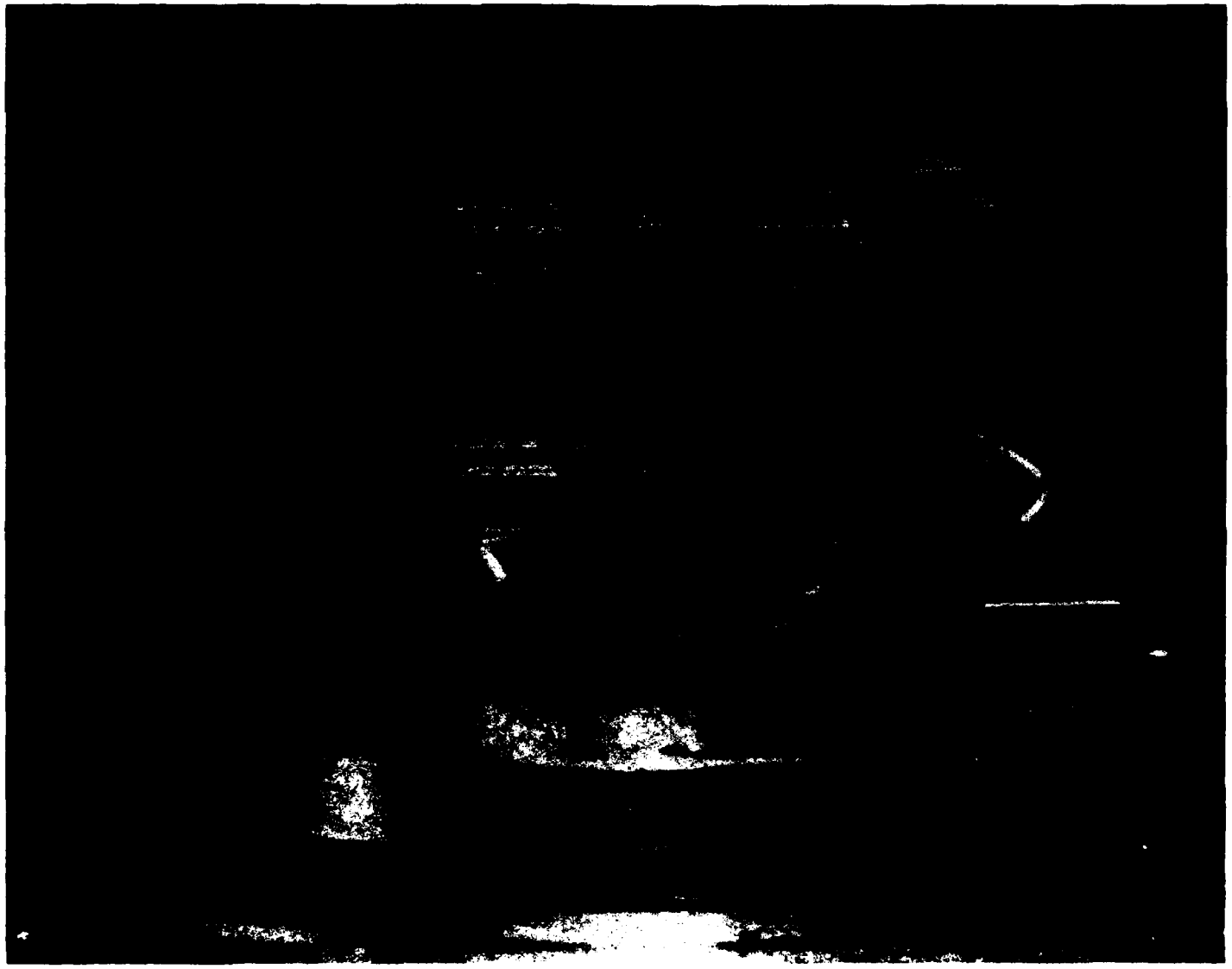

Fig. 11. Photograph of Detector Chamber and Detector Electrodes

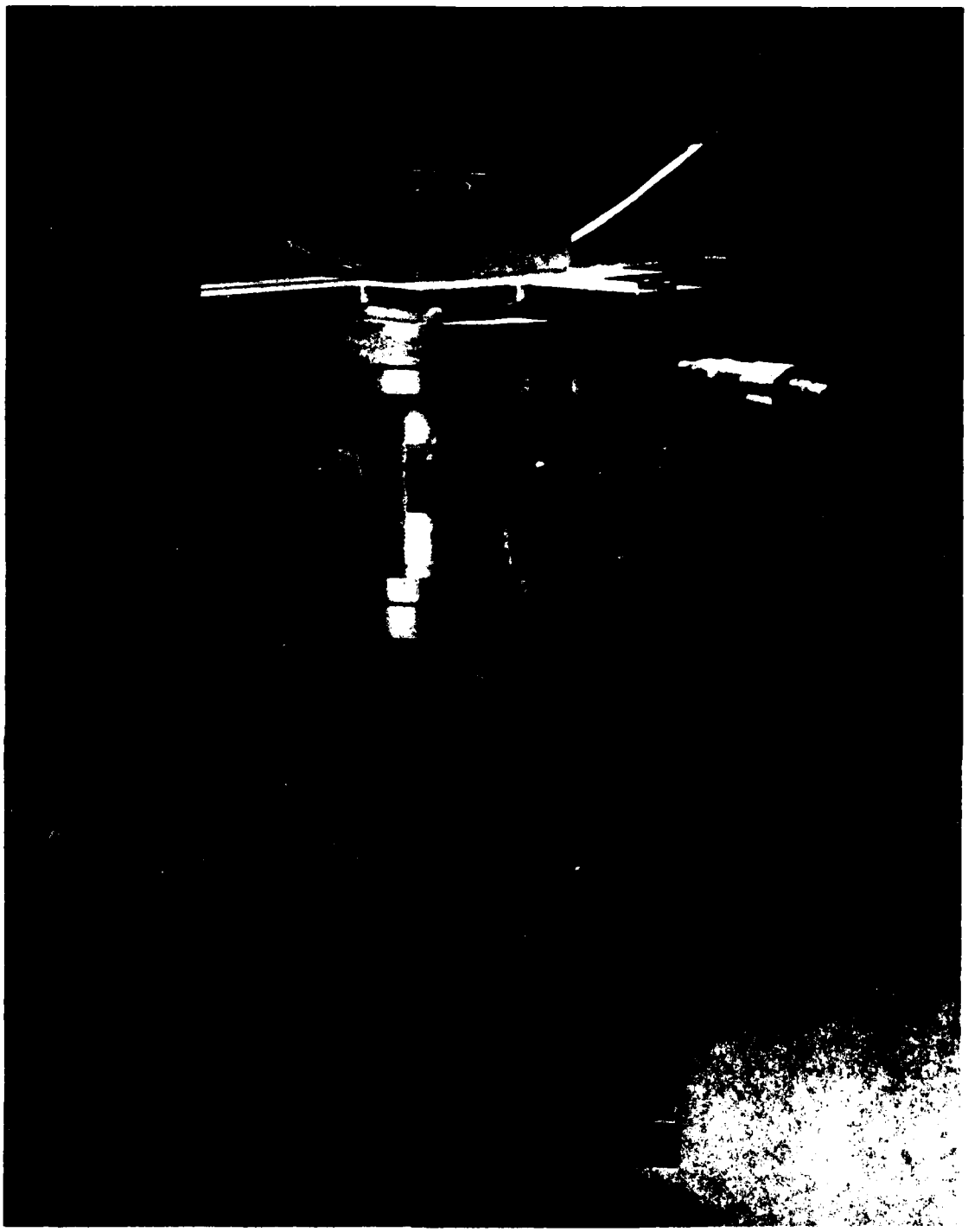

Fig. 12. Photograph of Wire Holder and Bath

V. EXPERIMENTAL RESULTS

Experiments were conducted using the x-ray generator, whose output is shown in Fig. 3. The purpose of the experiments was, first, to establish the validity of the calculations as a significant system design tool, and second, to obtain preliminary measurements on selected composite wires.

The electrode configuration for the detector has been illustrated in Fig. 11. The bath and wire positioning system are shown in Fig. 12. To establish some confidence in the calculations, it is appropriate to compare calculated and experimental values of the electrode current and the balance energy E_{max} for a known iodine concentration in the bath.

The bath liquids were the commercial contrast agents Renografin 60 and 76. These liquids contain 0.290 and 0.370 gm/cm^3 of iodine, respectively. In addition, center electrode current measurements were made for a 1.23-mm-thick sheet of aluminum used as an attenuator.

The results compared to the expected values of center electrode current measurements versus tube voltage are shown in Fig. 13. The measured currents agree very well with the predictions. We conclude from this that the calculations represent a valid design tool.

From measurements with the Renografin 60 and 76, as well as with the aluminum, effective attenuation coefficients based on the current measurements could be obtained for these substances. The results are shown in Fig. 14. They show that the two bath solutions do have effective attenuation coefficient vs E_{max} curves very much as illustrated in Fig. 7. The results are not sufficiently accurate in these preliminary measurements to say whether the aluminum curve corresponds to the Fig. 7(a) or 7(b) situation. Also, the iodine concentration that approximately balances the aluminum is somewhat below the values shown in Fig. 6. This is not really surprising as the bath solution is not simply water and iodine but contains a number of other chemicals. The most significant result is that the bath behaves qualitatively in the manner that was predicted.

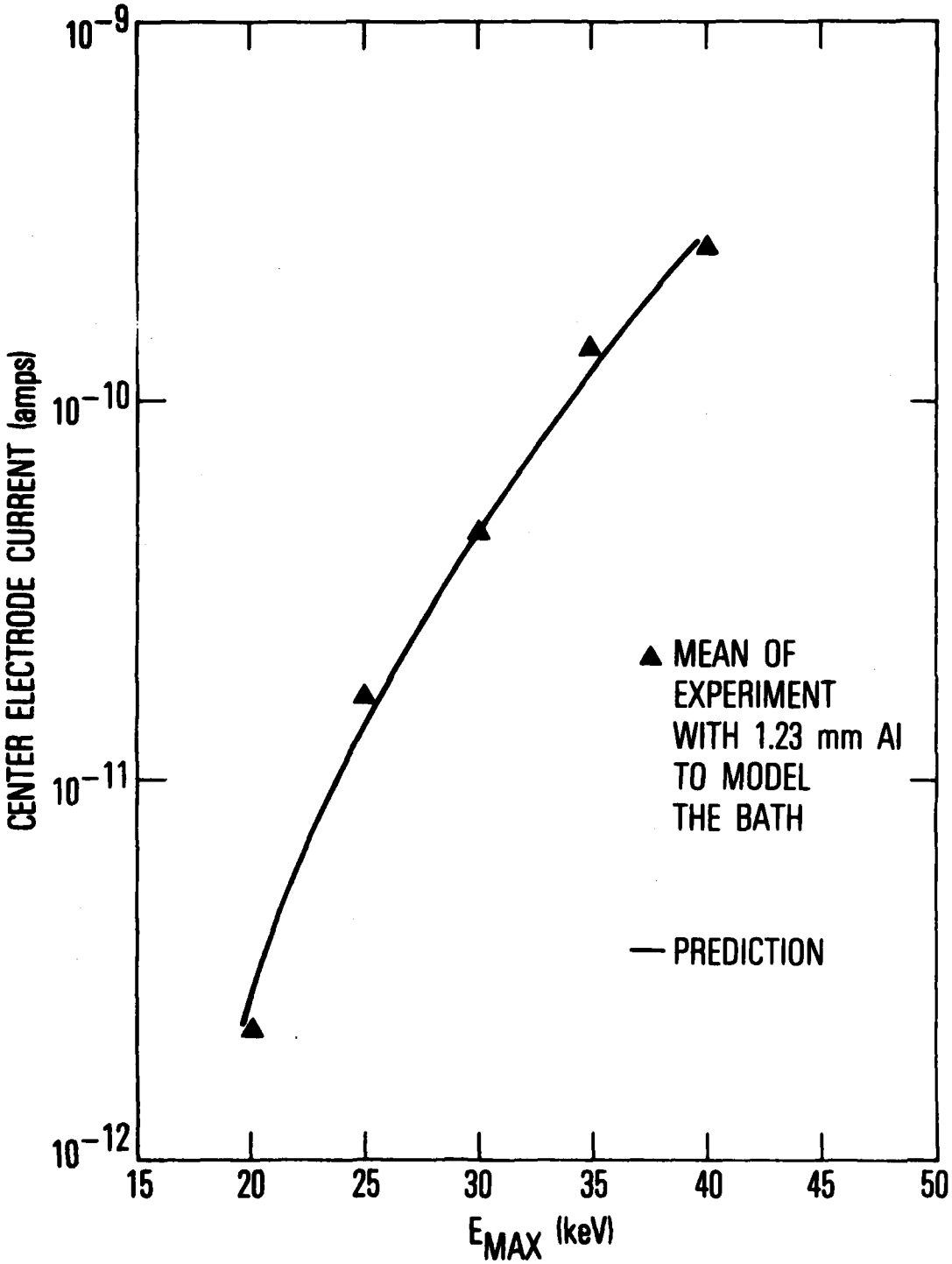

Fig. 13. Comparison of Preliminary Center Electrode Current Measurements and Predictions for Experimental Conditions

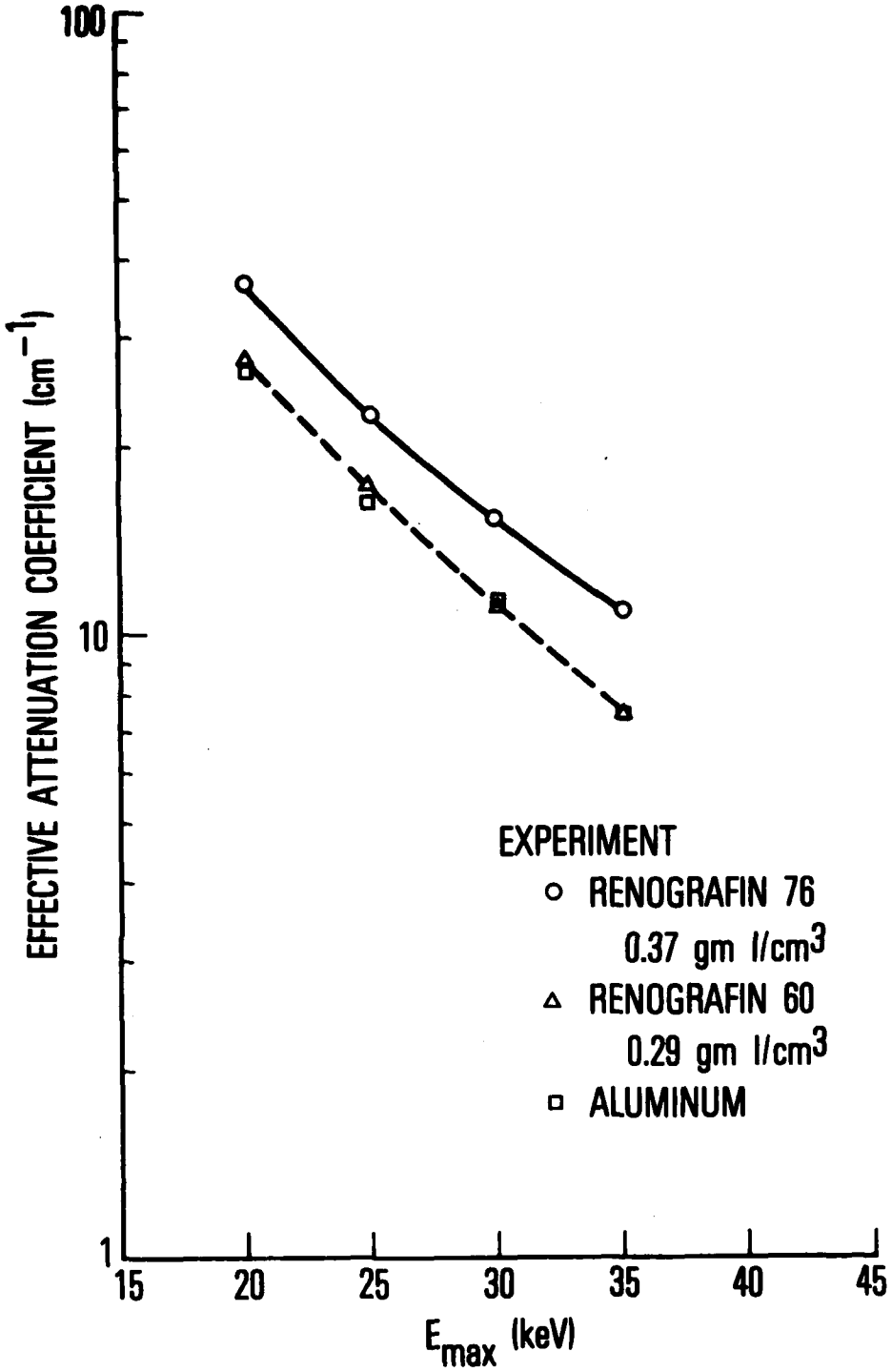

Fig. 14. Measured Effective Absorption Coefficients, using the Center Electrode Current, of Two Baths with Different Iodine Concentrations and of Aluminum

Some preliminary studies have been done on composite wires. A conventional film radiograph was taken of an aluminum wire, as well as "good" and "bad" composite wires. A set of microdensitometer traces of the film along an arbitrarily selected path perpendicular to the wires is shown in Fig. 15(a) and (b). In this figure, we present one set of traces with no bath fluid and another set with a bath that approximately balances the good wire. As is clear, there is a significant signal remaining at the position of the bad wire, which is of course the expected result.

Finally, detector dark currents were measured and found to be around 10^{-12} A. Detector noise injection does not appear to be a serious problem.

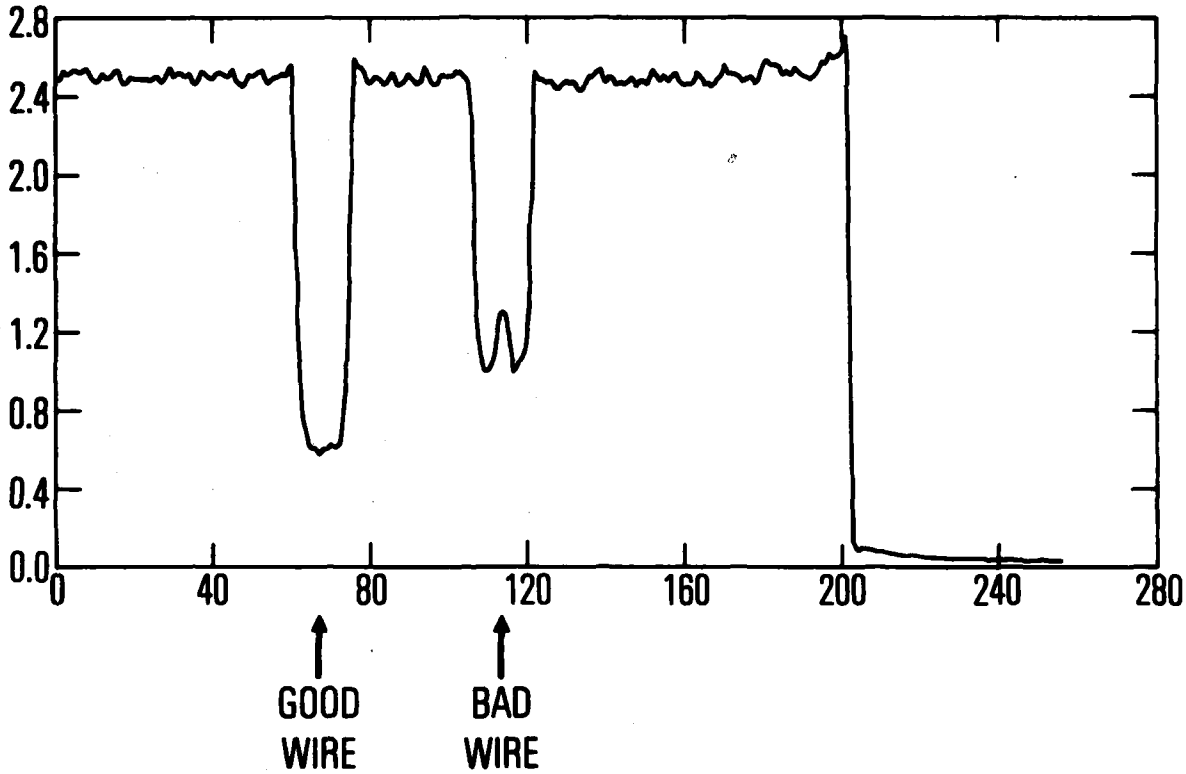

Fig. 15(a). Microdensitometer Trace of a Radiograph of a Good and Bad Wire with no Bath Fluid

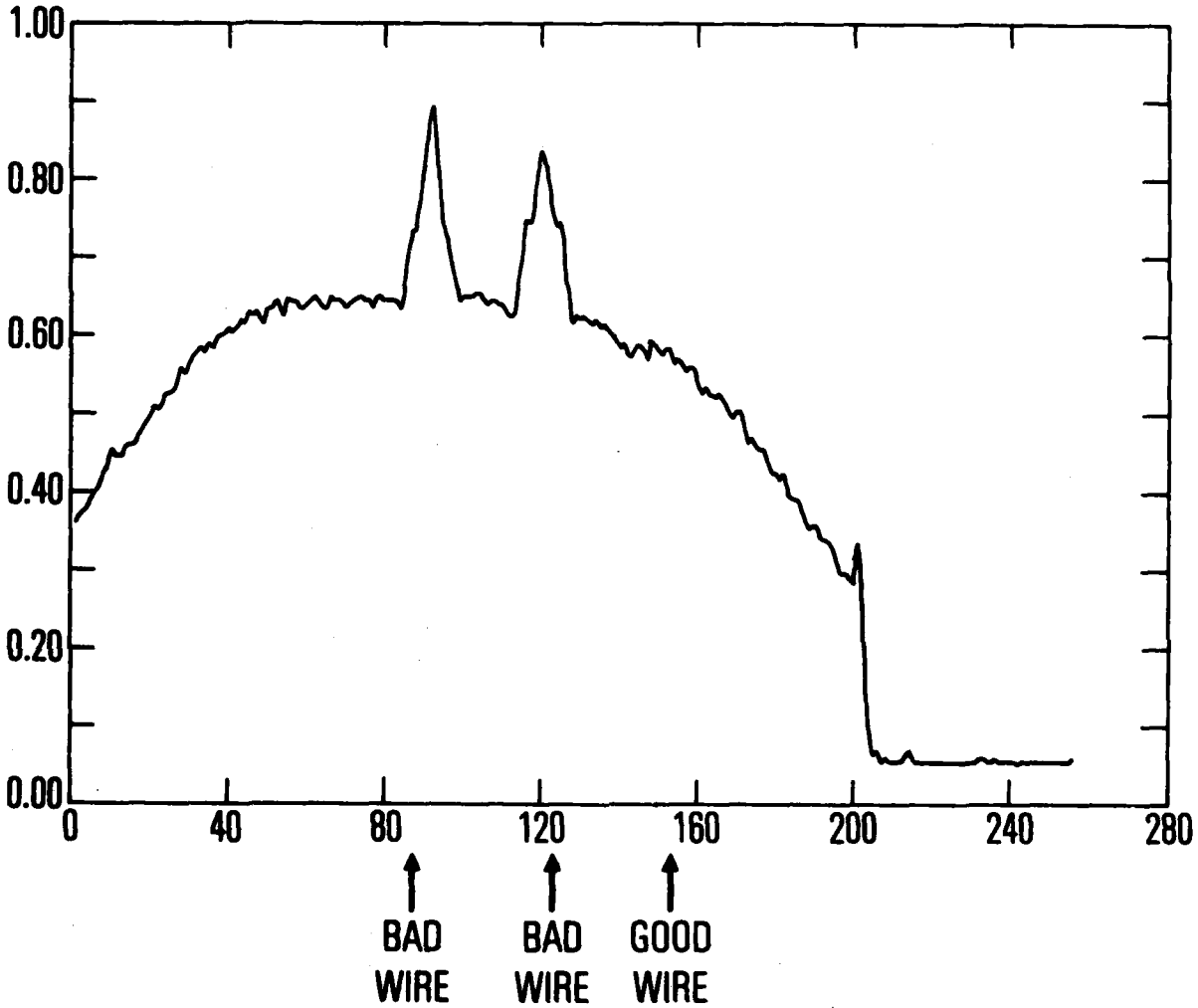

Fig. 15(b). Microdensitometer Trace of Two Bad Wires and One Good Wire in a Bath that just Balanced the Good Wire. The convex baseline is the result of bath depth changes caused by surface tension.

VI. CONCLUSIONS

Both calculations and preliminary experiments demonstrate that the proposed technique for detecting voids and composition anomalies in precursor composite wires is feasible. Using commercially available industrial x-ray sources with stationary, uncooled anodes, void fractions in the 1 to 3% range should be detectable at linear wire speeds of around 10 cm/sec. The resolution along the wire length would be about 1/2 cm. Higher linear speed or better length resolution would be possible with more powerful x-ray generators which are available.[9]

The bath immersion strategy appears to be a valid way of removing the uncertainties caused by geometric and physical property variations in graphite fiber, aluminum matrix composite wires.

REFERENCES

1. C. W. Anderson and G. V. Blessing, "Detection of Material Defects in Graphite-Reinforced Aluminum," NSWC TR 79-222, Naval Surface Weapons Center, 1979.

2. E. P. Muntz, Analysis of the Significance of Scattered Radiation in Reduced Dose Mammography, Med. Phys. 6:(2)110 (1979).

3. E. P. Muntz, A. Proudian, and P. B. Scott, "Radiographic System with Xerographic Printing," U. S. Patent 3,774,029 (1973).

4. E. P. Muntz, J. Lewis, and T. Azzarelli, On the Characteristics of Electron Radiographic Images in Diagnostic Radiology, in: "Medical X-ray Photo-Optical System Evaluation," 56, 208, SPIE Seminar Proceedings (1974).

5. A. Fenster, D. Plewes, and H. E. Johns, Efficiency and Resolution of Ionography in Diagnostic Radiology, Med. Phys. 1:(1)1 (1974).

6. G. T. Barnes, Characteristics of Scatter, in: "Reduced Dose Mammography," W. W. Logan and E. P. Muntz, eds., Masson, N.Y. (1979).

7. M. M. Ter-Pogossian, "The Physical Aspects of Diagnostic Radiology," Harper and Row, New York (1969).

8. H. E. Johns and J. R. Cunningham, "The Physics of Radiology," C. C. Thomas, Springfield, Ill. (1974).

9. T. R. Fewell and R. E Shuping, "Handbook of Mammographic X-ray Spectra," HEW 79-8071, U. S. D. H. E. W. Publication (1979).

10. K. R. Peschmann and G. Grosche, Amplification and Entailed Resolution Degradation in High Pressure Gas Ionography, Med. Phys. 4:(3)202 (1977).

11. L. A. Lehmann, R. E. Alvarez, A. Macovski, W. R. Brody, N. J. Pelc, S. J. Riederer, and A. J. Hall, Generalized Image Combination in Dual kVp Digital Radiography, Med. Phys. 8:(5)659 (1981).

12. J. H. Hubbell, "Photon Cross Sections, Attenuation Coefficients and Energy Absorption Coefficients from 10 keV to 100 GeV," NSRDS-NBS 29, U. S. Government Printing Office, Washington, D.C. (1969).

13. E. F. Christensen, T. S. Curry, and J. E. Dowdey, "An Introduction to the Physics of Diagnostic Radiology," Chapter 24, Lea and Febiger, Philadelphia (1978).

14. R. F. Wagner and E. P. Muntz, Intensifying Screens and Electrostatic Imaging in Mammography: Information and Display Parameters, in: "Reduced Dose Mammography," W. W. Logan and E. P. Muntz, eds., Masson, N.Y. (1979).

U.S. GOVERNMENT PRINTING OFFICE: 1983-783-004/2107-175

LABORATORY OPERATIONS

The Laboratory Operations of The Aerospace Corporation is conducting experimental and theoretical investigations necessary for the evaluation and application of scientific advances to new military space systems. Versatility and flexibility have been developed to a high degree by the laboratory personnel in dealing with the many problems encountered in the nation's rapidly developing space systems. Expertise in the latest scientific developments is vital to the accomplishment of tasks related to these problems. The laboratories that contribute to this research are:

Aerophysics Laboratory: Launch vehicle and reentry aerodynamics and heat transfer, propulsion chemistry and fluid mechanics, structural mechanics, flight dynamics; high-temperature thermomechanics, gas kinetics and radiation; research in environmental chemistry and contamination; cw and pulsed chemical laser development including chemical kinetics, spectroscopy, optical resonators and beam pointing, atmospheric propagation, laser effects and countermeasures.

Chemistry and Physics Laboratory: Atmospheric chemical reactions, atmospheric optics, light scattering, state-specific chemical reactions and radiation transport in rocket plumes, applied laser spectroscopy, laser chemistry, battery electrochemistry, space vacuum and radiation effects on materials, lubrication and surface phenomena, thermionic emission, photosensitive materials and detectors, atomic frequency standards, and bioenvironmental research and monitoring.

Electronics Research Laboratory: Microelectronics, GaAs low-noise and power devices, semiconductor lasers, electromagnetic and optical propagation phenomena, quantum electronics, laser communications, lidar, and electro-optics; communication sciences, applied electronics, semiconductor crystal and device physics, radiometric imaging; millimeter-wave and microwave technology.

Information Sciences Research Office: Program verification, program translation, performance-sensitive system design, distributed architectures for spaceborne computers, fault-tolerant computer systems, artificial intelligence, and microelectronics applications.

Materials Sciences Laboratory: Development of new materials: metal matrix composites, polymers, and new forms of carbon; component failure analysis and reliability; fracture mechanics and stress corrosion; evaluation of materials in space environment; materials performance in space transportation systems; analysis of systems vulnerability and survivability in enemy-induced environments.

Space Sciences Laboratory: Atmospheric and ionospheric physics, radiation from the atmosphere, density and composition of the upper atmosphere, aurorae and airglow; magnetospheric physics, cosmic rays, generation and propagation of plasma waves in the magnetosphere; solar physics, infrared astronomy; the effects of nuclear explosions, magnetic storms, and solar activity on the earth's atmosphere, ionosphere, and magnetosphere; the effects of optical, electromagnetic, and particulate radiations in space on space systems.

END

FILMED

1-84

DTIC